BILINGUAL PUBLISHING GROUP

Journal of Environmental & Earth Sciences

https://journals.bilpubgroup.com/index.php/jees

ARTICLE

Stochastic Analysis and Modeling of Velocity Observations in Turbulent Flows

***Evangelos Rozos*[1*], *Jorge Leandro*[2], *Demetris Koutsoyiannis*[3]**

[1] *Institute for Environmental Research & Sustainable Development, National Observatory of Athens, Athens, 15236, Greece*

[2] *Research Institute for Water and Environment, University of Siegen, Siegen, 57076, Germany*

[3] *Department of Water Resources and Environmental Engineering School of Civil Engineering, National Technical University of Athens, Athens, 15780, Greece*

ABSTRACT

Highly turbulent water flows, often encountered near human constructions like bridge piers, spillways, and weirs, display intricate dynamics characterized by the formation of eddies and vortices. These formations, varying in sizes and lifespans, significantly influence the distribution of fluid velocities within the flow. Subsequently, the rapid velocity fluctuations in highly turbulent flows lead to elevated shear and normal stress levels. For this reason, to meticulously study these dynamics, more often than not, physical modeling is employed for studying the impact of turbulent flows on the stability and longevity of nearby structures. Despite the effectiveness of physical modeling, various monitoring challenges arise, including flow disruption, the necessity for concurrent gauging at multiple locations, and the duration of measurements. Addressing these challenges, image velocimetry emerges as an ideal method in fluid mechanics, particularly for studying turbulent flows. To account for measurement duration, a probabilistic approach utilizing a probability density function (PDF) is suggested to mitigate uncertainty in estimated average and maximum values. However, it becomes evident that deriving the PDF is not straightforward for all turbulence-induced stresses. In response, this study proposes a novel approach by combining image velocimetry with a stochastic model to provide a generic yet accurate description of flow dynamics in such applications. This integration enables an approach based on the probability of failure, facilitating a more comprehensive analysis of turbulent flows. Such an approach is essential for estimating both short- and long-term stresses on hydraulic constructions under assessment.

Keywords: Smart modeling; Turbulent flows; Data analysis; Stochastic analysis; Image velocimetry

*CORRESPONDING AUTHOR:
Evangelos Rozos, Institute for Environmental Research & Sustainable Development, National Observatory of Athens, Athens, 15236, Greece; Email: erozos@noa.gr

ARTICLE INFO
Received: 4 December 2023 | Revised: 29 January 2023 | Accepted: 20 February 2023| Published Online: 5 March 2024
DOI: https://doi.org/10.30564/jees.v6i1.6109

CITATION
Rozos, E., Leandro, J., Koutsoyiannis, D., 2024. Stochastic Analysis and Modeling of Velocity Observations in Turbulent Flows. Journal of Environmental & Earth Sciences. 6(1): 45–56. DOI: https://doi.org/10.30564/jees.v6i1.6109

1. Introduction

Highly turbulent flows exhibit complex behavior, characterized by rapid and irregular fluctuations in velocity, pressure, and other flow parameters [1]. Many hydraulic structures and systems, such as piers, dams, channels, pipelines, and pumps, are susceptible to high-intensity turbulent flows [2]. Knowledge of turbulent flow characteristics helps in assessing the hydraulic loads, including pressure fluctuations, impacts, and dynamic forces, acting on structures. This information is crucial for ensuring the structural integrity, stability, and safety of hydraulic constructions under various flow conditions. For this reason, various numerical methods, such as the large eddy and the direct numerical simulation, have been developed to study turbulent flows [3]. However, turbulent flows often involve gas-liquid interfaces, which significantly increase the complexity of flow descriptions and can challenge even the most sophisticated numerical models [4]. For this reason, more often than not, scale models of hydraulic systems are built to study turbulent flows. Nevertheless, the monitoring of these physical models, even within meticulously controlled environments, is a laborious and demanding task.

Turbulent flows pose inherent challenges in flow measurement due to their unpredictable fluctuations and irregular nature. Conventional mechanically-based methods and acoustic Doppler velocimeters often introduce disturbances to the flow, making accurate measurements difficult. While there are intrusive methods available that can provide reliable measurements of high frequency with minimal flow disturbance, they are limited in their ability to obtain simultaneous measurements at multiple locations [5,6]. On the other hand, image velocimetry has been widely suggested by researchers as a non-intrusive method that offers accurate and reliable measurements of flow in both natural [7,8] and man-made hydraulic structures [9].

Image velocimetry stands out as an exceptionally well-suited method for studying turbulent flows, offering distinct advantages over traditional techniques such as current meters and acoustic Doppler velocimetry. One of its primary merits lies in its non-intrusive nature, allowing for flow measurements without physically disrupting the system under investigation. This characteristic is particularly crucial when studying turbulent flows, where the introduction of probes or other intrusive devices can alter the flow dynamics. Also, image velocimetry enables the determination of velocity fields with high temporal and spatial resolution, providing a detailed and comprehensive view of the turbulent characteristics, and for this reason, has gained significant popularity in hydraulic laboratories [2,10].

Image velocimetry can be based on different methods of video analysis, including approaches based on correlation, feature-tracking, or optical-flow analysis. Correlation-based techniques, such as Particle Image Velocimetry (PIV), rely on tracking the movement of identifiable features or particles in consecutive images [11]. Feature/particle tracking methods (PTV) focus on tracking specific features or points of interest in the flow field across multiple frames to track the movement of features and estimate the flow velocities [12]. In space-time image velocimetry (STIV) a search line of arbitrary length is set in the mainstream direction of the image, and the flow velocity is calculated from the gradient of the striped pattern that appears in the space-time image generated by stacking the image intensity information in the time direction [13]. Lastly, optical flow (OF) methods provide estimates of pixel or image region motion between consecutive frames, based on inverse methods applied to brightness variations in the image sequence [7]. Depending on the employed inverse method, there are different alternatives for the optical flow (OF) algorithms, such as the Horn-Schunk method, Lucas-Kanade method, and Farneback method [14].

PIV and OF have emerged as the most suitable methods for turbulent flows. PIV's capability to capture detailed flow phenomena, including wall-normal vortices and low-speed streaks, has been demonstrated, offering pivotal information to

understand underlying turbulence statistics such as streamwise velocity fluctuations, turbulence intensities, and Reynolds shear stress. This elucidates peak values and their locations near solid flow boundaries. PIV has served as an indispensable tool in studying bed shear stress from remotely measured surface turbulent dissipation fields in open channel flows [15]. On the other hand, the OF method, specifically employing the Farneback algorithm, provides denser spatial resolution and increased computational efficiency. This allows researchers to characterize the behavior of turbulent flow, and observe the formation of eddies, turbulent structures, and surface features like bumps and dimples [16].

Regarding the study of the impact of turbulent flows on nearby hydraulic structures, understanding Reynolds stresses and drag force is pivotal [17]. Typically, these stresses are estimated by the quantities $v_x'^2$, $v_x' \cdot v_y'$, and v_x^2, respectively, where v_x and v_y are the velocity vector components at a specific point of the flow field, and $v_x' = v_x - \langle v_x \rangle$ and $v_y' = v_y - \langle v_y \rangle$. The typical approach to obtaining foundational insights is to use the time-averaged values $\langle v_x'^2 \rangle$ and $\langle v_x' \cdot v_y' \rangle$ for the Reynolds stresses, and the maximum value, $\max(v_x^2)$, for the drag force. However, if the aforementioned quantities are obtained from observations of short time durations, the limitations of this approach become apparent when considering potential impacts over extended periods, where significantly larger magnitudes compared to the previously mentioned time-averaged and maximum values may emerge. Recognizing these limitations, a transition to a more comprehensive perspective becomes imperative. In this context, utilizing a probabilistic framework not only offers insights into dynamic behavior but also facilitates the analysis of stresses. This has been highlighted by scholars who suggest proceeding from Reynolds stress to PDF level of description [17]. Assuming v_x follows a normal distribution, the quantities $v_x'^2$ and v_x^2, representing the Reynolds normal stress and the drag force respectively, are expected to adhere to a central and non-central chi-square distribution respectively, with one degree of freedom [18]. In cases where the standard deviation is not 1, variable substitution is required [19].

As the probabilistic framework adeptly addresses normal stress, the complexity deepens when examining shear stress, specifically the product $v_x' \cdot v_y'$. In contrast to normal stress, where a closed-form solution aligns with the non-central chi-square distribution, for shear stress deriving the distribution of the product of the two random dependent variables, $v_x' \cdot v_y'$, is a formidable mathematical challenge [20,21]. An alternative practical approach is the utilization of a numerical stochastic model to navigate the intricacies of this product distribution. A multivariate stochastic model could be used to generate synthetic time series of velocity at various locations in the flow field. Subsequently, the corresponding values of Reynolds stresses and drag force could be estimated using the formulas mentioned earlier. Finally, by applying an empirical distribution to these time series, one could obtain the probability of exceedance.

Analyzing turbulent flows using image velocimetry yields vast datasets, demanding a nuanced approach to ensure statistically consistent results. The necessity to filter out spurious velocities further emphasizes the need for a methodologically rigorous framework. Moreover, the simultaneous monitoring of multiple locations introduces a layer of complexity that warrants a comprehensive probabilistic perspective. A stochastic model not only facilitates the probabilistic assessment of extreme velocity occurrences but also provides a systematic means to tackle the intricacies of the distribution of the product $v_x' \cdot v_y'$. At the same time, the stochastic model serves as a statistical filter to manage spurious velocities, ensuring that the obtained data reflects the true nature of turbulent flows.

In this study, we demonstrate the efficacy of integrating an image velocimetry algorithm with a stochastic model to address the previously mentioned challenges posed by turbulent flows. By harnessing the power of image velocimetry for non-intrusive, simultaneous measurements at multiple locations, and coupling it with a robust stochastic framework,

we aim to provide a comprehensive understanding of turbulent flow dynamics. This holistic approach not only enables a probabilistic assessment of extreme velocity values but also navigates the complexities associated with drag force, and shear and normal stresses calculations. It should be noted that the application of stochastic models to turbulent flows has been suggested by various researchers [22,23]. However, unlike these previous studies, which employed a stochastic approach to enhance the accuracy of numerical modeling, our study takes a distinctive approach. We utilize a stochastic model not only to improve the analysis of image velocimetry data but also to provide a probabilistic assessment of the stress factors arising from the intense and highly varying flow conditions. This dual application sets our study apart, allowing for a more comprehensive understanding of turbulent flow dynamics and its implications for hydraulic structures.

2. Materials and methods

2.1 Case study—hydraulic jump

A hydraulic jump serves as a compelling example of localized turbulent flow. When supercritical flow abruptly transitions to subcritical flow, a surge of kinetic energy is dissipated, causing a sudden increase in turbulence within the jump region. This localized turbulence is characterized by rapid fluctuations in velocity and pressure. The intensified turbulent flow can induce dynamic hydraulic loads on adjacent structures, such as embankments or bridge foundations, potentially jeopardizing their stability and integrity. The energy dissipation inherent in hydraulic jumps makes them (the adjacent structures) particularly prone to erosive forces, which, coupled with the turbulent nature of the flow, can lead to the scouring of riverbeds and banks.

Understanding the dynamics of turbulent flow within hydraulic jumps is crucial for assessing the potential impacts on nearby constructions and implementing effective engineering solutions to mitigate risks and ensure the longevity and safety of hydraulic infrastructure. For this reason, in this study, we have chosen this characteristic case of turbulent flow to demonstrate our methodology, i.e., analyze the video of a hydraulic jump with image velocimetry and then process the obtained time series with a stochastic model.

The video used in this study was obtained from the supplementary material of the publication of Mortazavi et al. [3]. This video represents a hydraulic jump with inflow Froude number of 2, Weber number of 1820 and density ratio of 831. The video has 598 frames, a frame rate of 24 fps, and a resolution of 960 × 540 px. The first frame of this video is displayed in **Figure 1**.

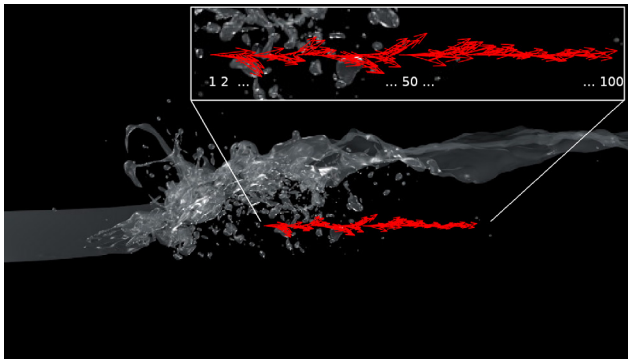

Figure 1. The vectors of the time-averaged velocities along the 100 points of the track line (marked by the origins of the vectors) are processed by the image velocimetry. The upper window is a zoom-in around the track line.

In this study, the Free-LSPIV particle image velocimetry algorithm [24–26] was used. Particle image velocimetry (other image velocimetry variants include particle tracking, space-time, optical flow etc. [27]) is based on the assumption that the most probable displacement of the particles within a flow captured in two subsequent frames of a video is the displacement that maximizes the correlation function. The process involves dividing the preceding frame into tiles, referred to as interrogation areas. Subsequently, these areas are compared for similarity (via the correlation function) with all subregions of the corresponding search areas, in the following frame. This enables a reliable estimation of motion yielding valuable insights into the velocity field of the fluid or particles under consideration [11].

The Free-LSPIV algorithm processes video

frames along a predefined track line, with an arbitrary number of points representing the centers of interrogation areas. Sequential runs of Free-LSPIV, each using different predefined track lines, can be employed to obtain velocities over a specific area of the flow. However, for this study, a single track line was utilized. The algorithm outputs velocity vectors at these points for the time intervals between the video frames. In this case study, velocity vectors were obtained at 100 points (**Figure 1**).

The data obtained by Free-LSPIV were stored in the 2D matrix $\boldsymbol{V}$ with dimensions nt × 2n. In this case, nt was 597 (representing the number of intervals between the 598 video frames), and n was 100 (indicating the number of points along the track line, as shown in **Figure 1**). This resulted in 200 columns of $\boldsymbol{V}$, which store the vector components along the principal flow directions (streamwise and vertical) for the 597 time steps. The matrix contained NaN (not a number) values corresponding to time instances and locations for which Free-LSPIV could not obtain velocity estimations due to the lack of distinct features (particles) in the specific locations of the corresponding frames.

Because some of the algorithms used in the analysis cannot handle NaN values (e.g., the fast Fourier transformation algorithm), 1D linear interpolations (applied separately for each column of the matrix $\boldsymbol{V}$) were used to fill the missing values.

2.2 Stochastic analysis of image velocimetry data

The stochastic model used in this study was a multivariate autoregressive of order 1. This is described by the following equation [28,29]:

$$\boldsymbol{v}_t = \boldsymbol{A}\,\boldsymbol{v}_{t-1} + \boldsymbol{B}\,\boldsymbol{\varepsilon}_t \tag{1}$$

$\boldsymbol{v}_t$ and $\boldsymbol{v}_{t-1}$ are 2n × 1 vectors of which elements are the transposed rows t and t–1 of the matrix $\boldsymbol{V}$, respectively, $\boldsymbol{A}$ is a 2n × 2n matrix, $\boldsymbol{\varepsilon}_t$ is a 2n × 1 vector with independent and identically distributed random numbers following the N(0,1) distribution, and $\boldsymbol{B}$ is a 2n × 2n matrix, where 2n is the number of the random variables (in this case, 2n equals 200 with the first 100 values corresponding to the streamwise vector components and the next 100 to the vertical vector components of the 100 points along the track line).

The matrices $\boldsymbol{A}$ and $\boldsymbol{B}$ can be calculated with the following formulas based on the available observations:

$$\boldsymbol{A} = \mathrm{cov}[\boldsymbol{V}, \boldsymbol{V}_1]\,(\mathrm{cov}[\boldsymbol{V}, \boldsymbol{V}])^{-1} \tag{2}$$

$$\boldsymbol{B}\boldsymbol{B}^{\mathrm{T}} = \mathrm{cov}[\boldsymbol{V}, \boldsymbol{V}] - \boldsymbol{A}\,\mathrm{cov}[\boldsymbol{V}, \boldsymbol{V}]\,\boldsymbol{A}^{\mathrm{T}} \tag{3}$$

where $\boldsymbol{V}_1$ is the vertical circular shift of $\boldsymbol{V}$ (the row t of $\boldsymbol{V}$ is the same as the row t+1 of $\boldsymbol{V}_1$).

The right-hand side of Equation (2) and Equation (3) can be computed directly from the data. However, a decomposition should be applied to the matrix obtained by the right-hand side of Equation (3) to obtain the matrix $\boldsymbol{B}$. In this study, the eigendecomposition method was employed [30]. According to this method, any square matrix, the right-hand side of Equation (3) in this case, that has eigenvalues λ_i and eigenvectors $\boldsymbol{z}_i$, i = 1, …, 2n, equals the product $\boldsymbol{Z}\,\boldsymbol{L}\,\boldsymbol{Z}^{-1}$, where $\boldsymbol{Z}$ is the 2n × 2n matrix with the eigenvectors $\boldsymbol{z}_i$ and $\boldsymbol{L}$ the 2n×2n diagonal matrix with its eigenvalues λ_i [31]. Since the right-hand side of Equation (3) is symmetric, the matrix $\boldsymbol{Z}$ is orthogonal (or orthonormal) [32], and hence $\boldsymbol{Z}^{-1} = \boldsymbol{Z}^{\mathrm{T}}$. If $\boldsymbol{L}^{0.5}$ is the matrix for which $\boldsymbol{L}^{0.5}\,\boldsymbol{L}^{0.5} = \boldsymbol{L}$, then Equation (3) becomes:

$$\boldsymbol{B}\boldsymbol{B}^{\mathrm{T}} = \boldsymbol{Z}\,\boldsymbol{L}\,\boldsymbol{Z}^{-1} = (\boldsymbol{Z}\,\boldsymbol{L}^{0.5})\,(\boldsymbol{L}^{0.5}\,\boldsymbol{Z})^{\mathrm{T}} \tag{4}$$

and therefore

$$\boldsymbol{B} = \boldsymbol{Z}\,\boldsymbol{L}^{0.5} \tag{5}$$

While various researchers have provided an intuitive description of the physical meaning of matrices $\boldsymbol{A}$ and $\boldsymbol{B}$, attributing the former to the strength of the influence of memory and the latter to the strength of randomness, concerns have been raised regarding the mathematical consistency of this definition, particularly with respect to the concept of "memory" [33].

Equation (1) applies to variables with a zero mean. Consequently, the observed time series should be standardized to have a zero mean before applying Equations (1) to (5). Subsequently, the generated time series from Equation (1) should be destandardized (by adding back the mean) to restore the intended statistical properties.

3. Results

The stochastic model described by Equation (1) was applied to produce 20000 × 200 synthetic velocity values (100 streamwise vector components and 100 vertical vector components at 20000-time steps). **Figure 2** displays the mean and standard deviation of the synthetic and observed velocity values at the 100 points along the track line. **Figure 3** displays the correlation coefficient between the streamwise components of the velocities at two subsequent points, and the correlation coefficient between the components of the velocity vector at all 100 points.

Figures 4 and 5 display the histogram and the second-order characteristics (the power spectrum and the climacogram) of the streamwise and vertical components of the velocity vector at the point $i = 50$ of the track line.

The red line in the power spectrum of **Figures 4 and 5** indicates the theoretically expected slope of –5/3 at the inertial sub-range, based on the Kolmogorov conceptual framework for turbulence [34]. The figures also provide the slope of the trend line that best fits the spectrum and the Hurst coefficient of the climacogram. The Hurst coefficient is related to the slope of the climacogram for the higher scales (or lower frequencies) according to the formula $H = 1 + \text{slope}/2$ [33].

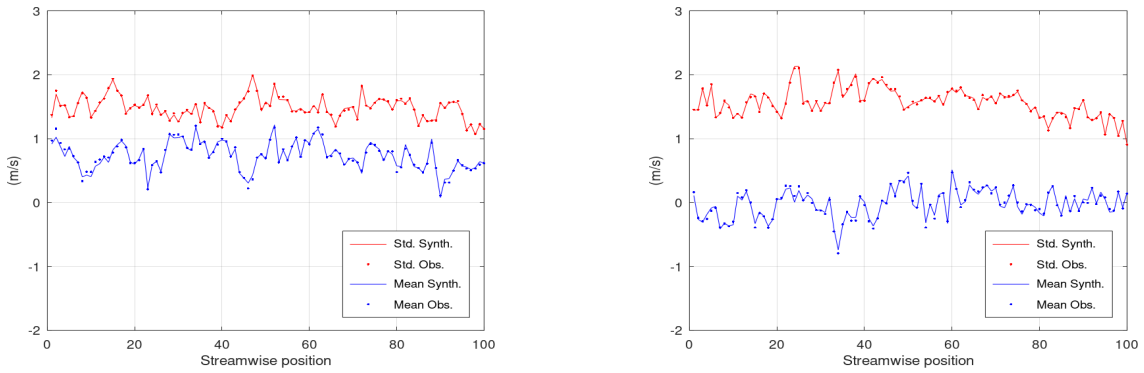

Figure 2. Comparison of the mean and standard deviation values of the observed and synthetic velocities at the 100 points of the track line; (A) mean and standard deviation values of the components of the velocity vectors along the streamwise direction, i.e., mean(v_{xi}) and std(v_{xi}), (B) mean and standard deviation values of the vertical components of the velocity vectors, i.e., mean(v_{yi}) and std(v_{yi}), where $i = 1, \ldots, 100$ in both (A) and (B).

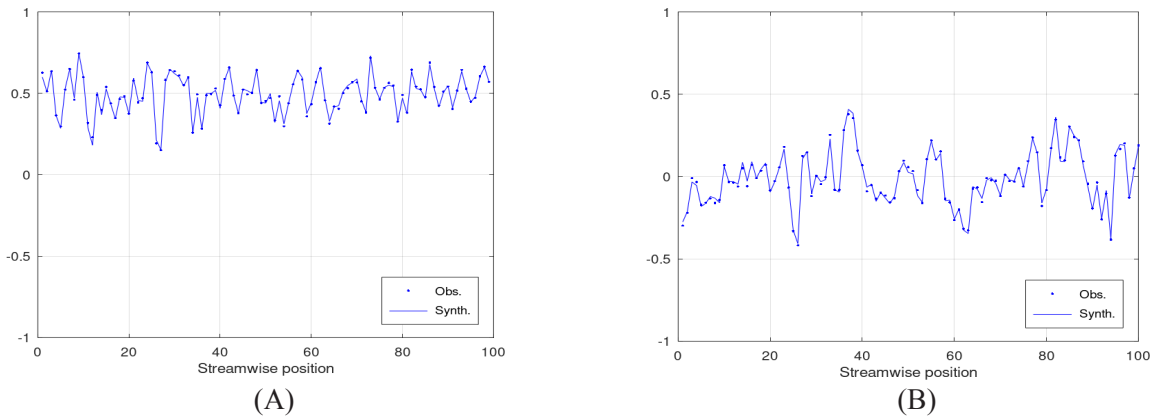

Figure 3. Comparison of the correlation coefficients of the observed and synthetic velocities at the 100 points of the track line; (A) $\rho(v_{xi}, v_{xi+1})$, where $i = 1, \ldots, 99$; (B) $\rho(v_{xi}, v_{yi})$, where $i = 1, \ldots, 100$.

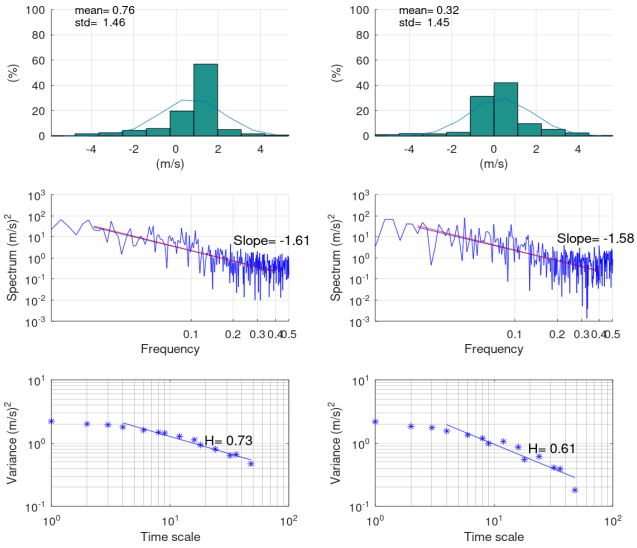

Figure 4. First- and second-order characteristics of the observed velocity (597 time steps) at point i = 50 of the track line. The left column corresponds to the streamwise component of the velocity vector and the right column corresponds to the vertical component.

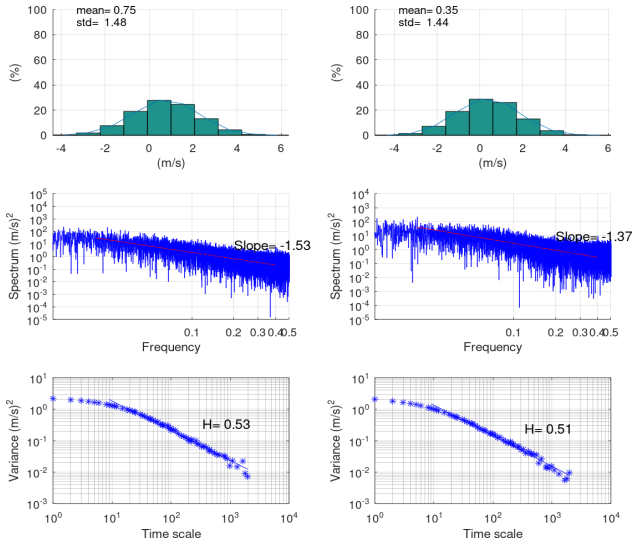

Figure 5. First- and second-order characteristics of the synthetic velocity (20000 time steps) at point i = 50 of the track line. The left column corresponds to the streamwise component of the velocity vector and the right column corresponds to the vertical component.

A collective comparison of the slope of the power spectrum of the observed and synthetic data is given in Table 1. The spectrum slope is estimated in the frequency region [0.02, 0.4] for all points of the track line. This region was selected because it gave the closest mean value to the expected theoretical, and at the same time the lowest standard deviation.

Table 1. The mean and the standard deviation of the 100 spectrum slopes of the velocity values at the 100 points along the track line.

	Mean	Standard deviation
Observed streamwise component	–1.68	0.21
Synthetic streamwise component	–1.66	0.20
Observed vertical component	–1.69	0.27
Synthetic vertical component	–1.66	0.22

A collective comparison of the H coefficient of the observed and synthetic time series is provided in **Table 2**.

Table 2. The mean and the standard deviation of the H coefficients of the two velocity vector components at the 100 points along the track line.

	Mean	Standard deviation
Observed streamwise component	0.70	0.078
Synthetic streamwise component	0.58	0.043
Observed vertical component	0.70	0.075
Synthetic vertical component	0.58	0.037

Figure 6 displays the return period plot of v_x^2, $v_x'^2$ and $|v_x' \cdot v_y'|$ at points i = 1 and 50 of the track line. The return period of a specific value is estimated with the formula $T/\Delta t = 1/(1 - P)$ [33], where Δt is the time step of the assessment, 1/24 second in this case, and P is the probability of non-exceedance of this specific value. The latter is estimated empirically with the Hazen plotting position, which is consistent with a set of statistical preconditions [35]. The probability of non-exceedance is estimated also for v_x^2 and $v_x'^2$ from the chi-square distribution with one degree of freedom.

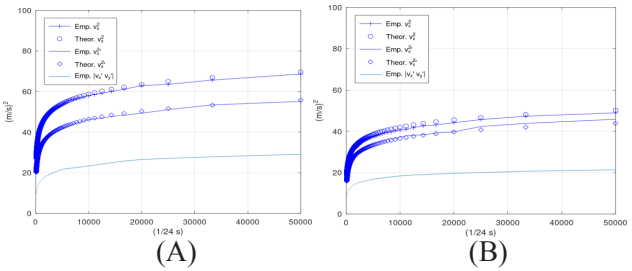

Figure 6. Return-period plot of v_x^2, $v_x'^2$ and $|v_x' \cdot v_y'|$ at points (A) i = 1, and (B) i = 50 of the track line.

4. Discussion

Figures 2 to 6 and **Tables 1 and 2**, featuring the

statistical metrics outlined in the preceding section, are dedicated to scrutinizing the effectiveness of the stochastic model in interpreting data acquired through the image velocimetry algorithm. The model showcased commendable performance in accurately capturing both first and select second-order statistics observed in the data. At all 100 points along the track line, it accurately reproduced the mean and standard deviation of the observed velocity time series, the correlation coefficient between the streamwise velocity components of two neighboring points, and the correlation coefficient between the two velocity components of any point. Yet, for this kind of application, it is crucial to ensure that the synthetic data manifests the distinctive statistical properties originating from the hydraulic conditions that define turbulent flows.

An essential characteristic of stochastic processes representing turbulent flows is the trend of the spectrum in the inertial sub-range of fully developed turbulence. Within this sub-range, smaller eddies transfer energy to larger eddies, creating a cascade of energy across various length scales. According to Kolmogorov, the spectrum in this sub-range tends to follow a power law with an exponent equal to –5/3 [34]. In our case study, the spectrum of both the synthetic and observed data demonstrated average slopes compatible with this power law in the frequency range [0.02, 0.4] (refer to **Figures 4 and 5**). Regarding the synthetic time series, this was encouraging since the mathematical analysis of autoregressive models, like the one used in this study, suggests that the log-log slope of the power spectrum of a time series produced with Equation (1) smoothly ranges from 0 for low frequencies to –2 for high frequencies, with the rate of decay determined by the values of the matrix $\boldsymbol{A}$ [33]. Noticeably, the average log-log slope of the synthetic time series in the inertial sub-range was virtually equal to the theoretically expected value of –5/3 (**Table 1**).

Another important characteristic of stochastic processes that represent turbulent flows is the long-term persistence, also known as Hurst-Kolmogorov (HK) behavior. The accurate representation of the HK dynamics is very important for assessing the hydraulic stresses induced by turbulent flows. According to Nordin et al. [36], the range of the cumulative sum of departures of any subset of the observed time series of the velocity of a turbulent flow with mean value u_{m} presents a scaling behavior according to the rule:

$$R \sim \sigma s^{H} \tag{6}$$

where σ is the standard deviation of the subset, s is the time scale or the subset length, H the Hurst coefficient, and $R = \max\{\Sigma_t\, u_t - t\, u_{\mathrm{m}}\} - \min\{\Sigma_t\, u_t - t\, u_{\mathrm{m}}\}$ with $t = 0, \ldots, s$. The value of R ranges from 0 to higher values, where 0 corresponds to a time series of a constant value. Higher values of R indicate both persistence and higher excursions from the mean value.

From Equation (6) it becomes evident that the Hurst coefficient plays an important role in the duration and magnitude of the deviations of the velocity from the mean value. According to **Table 2**, the average Hurst coefficient of the observed and synthetic velocities is 0.70 and 0.58 respectively. This deviation was expected because of the Markovian nature of the stochastic model employed in this study. The climacogram of the synthetic time series (**Figure 5**) exhibits the typical pattern of the climacogram of a Markovian process [33]. In this case study, the Hurst coefficient of the observed was relatively low. However, H values up to 0.9 are not uncommon in turbulent flows [37]. For such cases, a generalized Hurst-Kolmogorov stochastic model should be considered [1].

Figure 6 is the most important output of this study and could form the basis for a probabilistic assessment of the potential impacts of turbulent flow on nearby construction. The return period plots at points $i = 1$ and 50 provide a direct visual assessment of the stressful conditions at these assessed locations. The magnitude of the stresses decreases with distance from the hydraulic jump, which is manifested by the lowering of the curves.

Consider a scenario where the previous case study concerned the assessment of the stress on a

construction at point 1 of the track line. If the study was limited exclusively to the analysis of the data obtained by the image velocimetry method, the reported maximum v_x^2 value during the 25-second video recording period would be 34.87 $(m/s)^2$. However, there is no specific reason why the assessment period should be constrained to the duration of the video or the duration of any other monitoring procedure (e.g., the duration of sampling with a current meter). The assessed construction will remain subject to stresses for extended periods. Ideally, the stress values used for the design or the estimation of impacts on the construction should be based on the following formulation: given the expected duration $k\,\Delta t$ of a stressful event, and an acceptable probability of exceedance at least once during the assessed period (probability of failure) equal to R, what are the expected maximum stress values. The handling of this probabilistic formulation is as follows. Given the values of k and R, and by employing the probability of failure equation [38]:

$$R = 1 - (1 - \Delta t / T)^k \quad (7)$$

One could solve for T, and then from **Figure 6** obtain the estimation for the design values.

Figure 6 indicates that a stress level of 34.87 $(m/s)^2$ corresponds to a return period of 308 time steps (each time step being 1/24 second). This results in a relatively short duration of 13 seconds, which is notably shorter than the expected duration of high flows capable of inducing intense turbulence and increased stresses on a structure.

It should be noted that in a comprehensive study, **Figure 6** should also include the confidence limits of the return period plots [33]. This would require generating not a single, but a set of synthetic time series.

Future research could focus on alternative stochastic models to address various issues that were unveiled in this study.

• As mentioned previously, models that accurately represent the Hurst-Kolmogorov behavior should be assessed. This will enable the capture of this important second-order characteristic for reproducing the effect of persistence.

• The stochastic model used in this case study is 1D in the sense that the index set of the process concerns one dimension, the time in Equation (1). By extending the set to three dimensions, one could explore comprehensive spatio-temporal approaches, like those employed in geostatistics [39]. However, multidimensional modeling is challenging and, for this reason, is employed only in a small portion of stochastic model applications.

• The histograms in **Figure 4** suggest that some of the observed time series do not follow normal distribution. It should be noted that Equation (3) is an underdetermined system of equations, therefore Equation (5) is only one of the infinite alternative solutions. For example, Koutsoyiannis has suggested a solution of Equation (3) that preserves the skewness [28]. This may prove advantageous in cases where the distribution of the involved random variables is not Gaussian.

• An alternative coordinate system could be employed to express the velocity vector into scalar variables. For example, in weather forecast modeling they have suggested employing polar coordinates since with Cartesian coordinates there is an incentive to minimize the wind magnitude in the face of predictive uncertainty. Using polar coordinates, accounting for both magnitude and angular direction, may offer advantages in such instances [40].

5. Conclusions

In this study, we presented a novel approach that integrates image velocimetry with a stochastic model to comprehensively analyze turbulent flows, with a focus on hydraulic jumps as a characteristic case. The synergy of these methodologies allowed for a nuanced understanding of flow dynamics, offering insights that contribute to both hydraulic engineering and structure design.

The proposed stochastic model, a multivariate autoregressive model of order 1, demonstrated commendable performance in capturing statistical properties of turbulent flows. Through the analysis of synthetic and observed data, we observed the

model's ability to reproduce key characteristics of the statistical properties and structure.

The power law behavior in the inertial subrange of fully developed turbulence was verified, with the spectral analysis revealing an exponent close to the theoretical –5/3. This alignment with Kolmogorov's theory reaffirms the accuracy of the image velocimetry data and the stochastic model. Additionally, the study delved into the long-term persistence, or Hurst-Kolmogorov behavior, revealing insights into the scaling behavior of velocity deviations from mean values.

The significance of this work lies in its potential applications for assessing hydraulic stresses on nearby constructions in turbulent flow scenarios. By providing a probabilistic framework for extreme velocity values, the methodology presented here offers a valuable tool for hydraulic engineering practices. The return-period plot emerges as a pivotal output of the stochastic model, allowing for a probabilistic assessment of potential impacts on nearby constructions over extended durations.

In conclusion, the integrated approach presented in this study opens avenues for advancements in the field of turbulent flow analysis. By bridging image velocimetry and stochastic modeling, we not only validate the accuracy of our methodology but also contribute valuable insights that can inform the design, safety considerations, and risk assessments of hydraulic structures under diverse flow conditions. Moreover, the demonstrated efficacy of our integrated approach in hydraulic model experiments underscores its applicability in practical settings, enhancing the reliability and precision of flow analyses crucial for hydraulic engineering.

Author Contributions

Conceptualization, E.R. and D.K.; methodology, E.R.; software, E.R.; validation, J.L. and D.K.; formal analysis, E.R.; investigation, E.R.; resources, J.L.; data curation, E.R.; writing—original draft preparation, E.R.; writing—review and editing, J.L. and D.K.; visualization, E.R.; supervision, E.R.; project administration, E.R.

Conflict of Interest

The authors declare no conflict of interest.

Funding

This research received no external funding.

Acknowledgments

The authors wish to thank the Deutscher Akademischer Austauschdienst (DAAD) for covering the travel costs necessary for the completion of this study.

References

[1] Dimitriadis, P., Koutsoyiannis, D., Papanicolaou, P., 2016. Stochastic similarities between the microscale of turbulence and hydro-meteorological processes. Hydrological Sciences Journal. 61(9), 1623–1640.
DOI: https://doi.org/10.1080/02626667.2015.1085988

[2] Gautam, P., Eldho, T.I., Mazumder, B.S., et al., 2019. Experimental study of flow and turbulence characteristics around simple and complex piers using PIV. Experimental Thermal and Fluid Science. 100, 193–206.
DOI: https://doi.org/10.1016/j.expthermflusci.2018.09.010

[3] Mortazavi, M., Le Chenadec, V., Moin, P., et al., 2016. Direct numerical simulation of a turbulent hydraulic jump: Turbulence statistics and air entrainment. Journal of Fluid Mechanics. 797, 60–94.
DOI: https://doi.org/10.1017/jfm.2016.230

[4] Leandro, J., Carvalho, R., Chachereau, Y., et al., 2012. Estimating void fraction in a hydraulic jump by measurements of pixel intensity. Experiments in Fluids. 52, 1307–1318.
DOI: https://doi.org/10.1007/s00348-011-1257-1

[5] Murzyn, F. (editor), 2010. Assessment of different experimental techniques to investigate the hydraulic jump: do they lead to the same results. 3rd International Junior Researcher and

Engineer Workshop on Hydraulic Structures; 2010 May 4–6; Edinburgh, Scotland.

[6] Wang, H., Murzyn, F., 2017. Experimental assessment of characteristic turbulent scales in two-phase flow of hydraulic jump: from bottom to free surface. Environmental Fluid Mechanics. 17, 7–25.
DOI: https://doi.org/10.1007/s10652-016-9451-6

[7] Jyoti, J.S., Medeiros, H., Sebo, S., et al., 2023. River velocity measurements using optical flow algorithm and unoccupied aerial vehicles: A case study. Flow Measurement and Instrumentation. 91, 102341.
DOI: https://doi.org/10.1016/j.flowmeasinst.2023.102341

[8] Jin, T., Liao, Q., 2019. Application of large scale PIV in river surface turbulence measurements and water depth estimation. Flow Measurement and Instrumentation. 67, 142–152.
DOI: https://doi.org/10.1016/j.flowmeasinst.2019.03.001

[9] Emadzadeh, A., Chiew, Y.M. (editors), 2017. Bubble dynamics and PIV measurements in a hydraulic jump. The 37th IAHR World Congress; 2017 Aug 13–18; Kuala Lumpur, Malaysia.

[10] Ayegba, P.O., Edomwonyi□Otu, L.C., 2020. Turbulence statistics and flow structure in fluid flow using particle image velocimetry technique: A review. Engineering Reports. 2(3), e12138.
DOI: https://doi.org/10.1002/eng2.12138

[11] Fujita, I., Muste, M., Kruger, A., 1998. Large-scale particle image velocimetry for flow analysis in hydraulic engineering applications. Journal of hydraulic Research. 36(3), 397–414.
DOI: https://doi.org/10.1080/00221689809498626

[12] Fujita, I., Kawamura, Y. (editors), 2001. Discharge measurements of flood flow by imaging technology and float method. Proceedings of the 29th Congress of IAHR; 2001 Sep 16–21; Beijing, China.

[13] Watanabe, K., Fujita, I., Iguchi, M., et al., 2021. Improving accuracy and robustness of space-time image velocimetry (STIV) with deep learning. Water, 13(15), 2079.
DOI: https://doi.org/10.3390/w13152079

[14] Shi, R., Leng, X., Chanson, H., 2020. On optical flow techniques applied to breaking surges. Flow Measurement and Instrumentation. 72, 101710.
DOI: https://doi.org/10.1016/j.flowmeasinst.2020.101710

[15] Johnson, E.D., Cowen, E.A., 2017. Estimating bed shear stress from remotely measured surface turbulent dissipation fields in open channel flows. Water Resources Research. 53(3), 1982–1996.
DOI: https://doi.org/10.1002/2016WR018898

[16] Romagnoli, M., Carvalho, R., Leandro, J., 2013. Turbulence characterization in a gully with reverse flow. Journal of Hydraulic Engineering. 139(7), 736–744.
DOI: https://doi.org/10.1061/(ASCE)HY.1943-7900.0000737

[17] Pope, S.B., 2001. Turbulent flows. Measurement Science and Technology. 12(11).
DOI: https://doi.org/10.1088/0957-0233/12/11/705

[18] Papoulis, A., 1990. Probability and statistics. Prentice-Hall: New Jersey. pp. 219.

[19] Patnaik, P.B., 1949. The Non-Central χ2- and F-Distribution and their applications. Biometrika. 36 (½), 202–232.
DOI: https://doi.org/doi:10.2307/2332542

[20] Nadarajah, S., Pogány, T.K., 2016. On the distribution of the product of correlated normal random variables. Comptes Rendus. Mathématique. 354(2), 201–204.
DOI: https://doi.org/10.1016/j.crma.2015.10.019

[21] Cui, G., Yu, X., Iommelli, S., et al., 2016. Exact distribution for the product of two correlated Gaussian random variables. IEEE Signal Processing Letters. 23(11), 1662–1666.
DOI: https://doi.org/10.1109/LSP.2016.2614539

[22] Zare, A., Georgiou, T.T., Jovanović, M.R., 2020. Stochastic dynamical modeling of turbu-

lent flows. Annual Review of Control, Robotics, and Autonomous Systems. 3, 195–219. DOI: https://doi.org/10.1146/annurev-control-053018-023843

[23] Czibere, T., 2006. Calculating turbulent flows based on a stochastic model. Journal of Computational and Applied Mechanics. 7(2), 155–188.

[24] Rozos, E., Dimitriadis, P., Mazi, K., et al., 2020. On the uncertainty of the image velocimetry method parameters. Hydrology. 7(3), 65. DOI: https://doi.org/10.3390/hydrology7030065

[25] Rozos, E., Mazi, K., Koussis, A.D., 2021. Probabilistic evaluation and filtering of image velocimetry measurements. Water. 13(16), 2206. DOI: https://doi.org/10.3390/w13162206

[26] Rozos, E., Mazi, K., Lykoudis, S., 2022. On the accuracy of particle image velocimetry with citizen videos—five typical case studies. Hydrology. 9(5), 72. DOI: https://doi.org/10.3390/hydrology9050072

[27] Wijaya, F., Liu, W.C., Huang, W.C., 2023. Comparative assessment of different image velocimetry techniques for measuring river velocities using unmanned aerial vehicle imagery. Water. 15(22), 3941. DOI: https://doi.org/10.3390/w15223941

[28] Koutsoyiannis, D., 1999. Optimal decomposition of covariance matrices for multivariate stochastic models in hydrology. Water Resources Research. 35(4), 1219–1229. DOI: https://doi.org/10.1029/1998WR900093

[29] Matalas, N.C., 1967. Mathematical assessment of synthetic hydrology. Water Resources Research. 3(4), 937–945. DOI: https://doi.org/10.1029/WR003i004p00937

[30] Goodfellow, I., Bengio, Y., Courville, A., 2016. Deep learning. MIT Press: Cambridge. pp. 40.

[31] Rawlings, J.O., Pantula, S.G., Dickey, D.A., 1998. Applied regression analysis: A research tool. Springer: New York. pp. 58.

[32] Searle, S.R., 1982. Matrix algebra useful for statistics. John Wiley & Sons: New York.

[33] Koutsoyiannis, D., 2023. Stochastics of hydroclimatic extremes—A cool look at risk, edition 3. Kallipos Open Academic Editions: Athens. DOI: https://doi.org/10.57713/kallipos-1

[34] Biferale, L., Boffetta, G., Castaing, B., 2003. Fully developed turbulence. The Kolmogorov legacy in physics. Springer-Verlag: Heidelberg. pp. 149–172.

[35] Hyndman, R.J., Fan, Y., 1996. Sample quantiles in statistical packages. The American Statistician. 50(4), 361–365.

[36] Nordin, C.F., McQuivey, R.S., Mejia, J.M., 1972. Hurst phenomenon in turbulence. Water Resources Research. 8(6), 1480–1486. DOI: https://doi.org/10.1029/WR008i006p01480

[37] Dimitriadis, P., Papanicolaou, P. (editors), 2012. Statistical analysis of turbulent positively buoyant jets. European Geosciences Union General Assembly 2012; 2012 Apr 22–27; Vienna, Austria.

[38] Te Chow, V., Maidment, D.R., Mays, L.W., 1988. Applied hydrology. McGraw-Hill: New York.

[39] Kitanidis, P.K., 1993. Geostatistics. The handbook of hydrology. McGraw-Hill: New York.

[40] Lam, R., Sanchez-Gonzalez, A., Willson, M., et al., 2023. Learning skillful medium-range global weather forecasting. Science. 382(6677), 1416–1421. DOI: https://doi.org/10.1126/science.adi2336